PHYSICAL REVIEW B **84**, 125433 (2011)

Decoupling conservative and dissipative forces in frequency modulation atomic force microscopy

Aleksander Labuda,* Yoichi Miyahara, Lynda Cockins, and Peter H. Grütter
Department of Physics, McGill University, 3600 University, Montreal, Canada, H3A 2T8
(Received 1 June 2011; published 15 September 2011)

Experiments and theoretical calculations of conservative forces measured by frequency modulation atomic force microscopy (FM-AFM) in vacuum are generally in reasonable agreement. This contrasts with dissipative forces, where experiment and theory often disagree by several orders of magnitude. These discrepancies have repeatedly been attributed to instrumental artifacts, the cause of which remains elusive. We demonstrate that the frequency response of the piezoacoustic cantilever excitation system, traditionally assumed flat, can actually lead to surprisingly large apparent damping by the coupling of the frequency shift to the drive-amplitude signal, typically referred to as the "dissipation" signal. Our theory predicts large quantitative and qualitative variability observed in dissipation spectroscopy experiments, contrast inversion at step edges and in atomic-scale dissipation imaging, as well as changes in the power-law relationship between the drive signal and bias voltage in dissipation spectroscopy. The magnitude of apparent damping can escalate by more than an order of magnitude at cryogenic temperatures. We present a simple nondestructive method for correcting this source of apparent damping, which will allow dissipation measurements to be reliably and quantitatively compared to theoretical models.

DOI: 10.1103/PhysRevB.84.125433 PACS number(s): 68.37.Ps, 07.79.Lh

I. INTRODUCTION

Since its invention in 1991, frequency modulation atomic force microscopy[1] (FM-AFM) has proven to be an indispensable method for probing forces at the atomic scale in vacuum environments. The heart of the instrument is a cantilever that is self-excited at its natural frequency, which shifts upon interaction with a sample under study. The cantilever oscillation amplitude is kept constant by an automatic-gain-controller (AGC), which adjusts the amplitude of the drive signal used to actuate the cantilever by piezoacoustic excitation. One nominal advantage of FM-AFM over other techniques is the decoupling of conservative and dissipative forces: the shift of the self-excited oscillation frequency is proportional to the effective interaction stiffness,[2] while the drive amplitude of the AGC directly relates to the interaction damping with negligible coupling between both signals.[3,4] This situation *should* greatly simplify the interpretation of data acquired by FM-AFM.

The unprecedented understanding and control of tip-sample conservative forces in FM-AFM has enabled impressive room-temperature manipulation of single atoms[5] and chemical identification of individual surface atoms,[6] for example. On the other hand, the poorly understood dissipation measurements using FM-AFM have mainly been the source of questions[7] and controversies.[8,9]

Dissipation contrast mechanisms in FM-AFM have been extensively studied from both experimental[10–17] and theoretical[18–28] perspectives. Although most postulated dissipation mechanisms have been experimentally verified, the variability in the data often exceeds theoretical predictions by orders of magnitude.[29,30] The large discrepancies between theory and experiment have led to the notion of "apparent damping"—also known as "apparent dissipation."[31] It refers to any change in the drive amplitude that is not related to tip-sample dissipative forces; rather, it is assumed to be caused by nonideal behavior of the instrument. Despite numerous investigations,[11,29,32] the large variability in experimental observations remains elusive.

At the forefront of nanoscience, many experiments performed at cryogenic temperatures identify theoretically predicted physical processes with FM-AFM dissipation measurements. The degenerate energy-level structure in quantum dots was identified by measuring the amplitude dependence of dissipation.[33–35] The suppression of electronic friction on Nb films in the superconducting state was identified by a change in the power law between the dissipation and bias voltage ($V^2 \rightarrow V^4$).[36] The chemical identification of tip-apex termination[37] and recognition of atomic species at semiconductor surfaces[38] are aided by measurements of single atomic-contact adhesion studied by dissipation-distance spectroscopy.

Our detailed analysis of FM-AFM clearly demonstrates that drawing robust conclusions from dissipation experiments requires an accurate measurement of the transfer function of the piezoacoustic excitation system used to oscillate the cantilever. Omitting this measurement can lead to false interpretation of changes in the drive signal, which relate to the physics of the FM-AFM system as opposed to tip-sample physics. For example, the piezoacoustic transfer function can cause contrast inversion at step edges or in atomic contrast in dissipation images, as well as change the dependence between the drive signal and bias voltage from quadratic to quartic, or completely distort dissipation-distance spectroscopy results both quantitatively and qualitatively. Notably, although the piezoacoustic transfer function affects measurements performed at any temperature, it becomes exceedingly problematic at cryogenic temperatures at which sensitive dissipation experiment are being performed.

In this study, we discuss the apparent damping caused by the piezoacoustic excitation transfer function. Recent communications[39,40] have derived theories and methods for eliminating this source of apparent damping in air and liquid environments. Here, we present a theory tailored for vacuum environments, demonstrate a noninvasive method for its implementation, and assess its impact on a wide range of dissipation experiments at different temperatures.

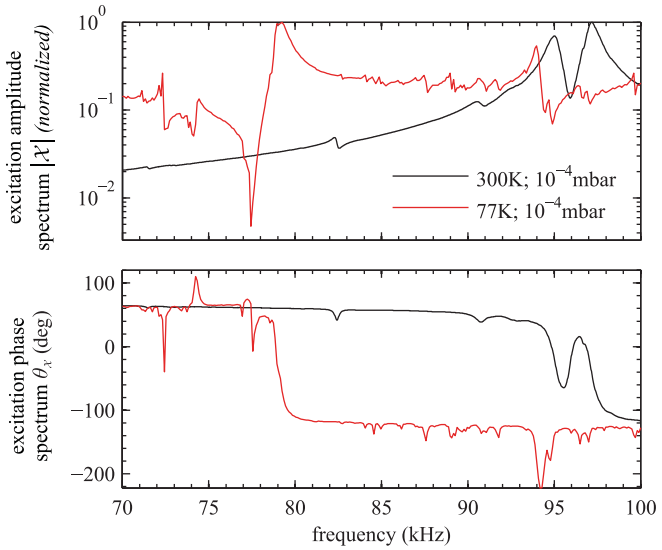

FIG. 1. (Color online) The amplitude $|\mathcal{X}|$ and phase $\theta_{\mathcal{X}}$ components of the piezoacoustic excitation transfer function $\mathcal{X}(\omega)$ acquired at two different temperatures. This measurement was obtained by piezoacoustically driving a cantilever well below its resonance frequency (∼160 kHz) and detecting its response with a lock-in amplifier across [70, 100] kHz. The mechanical cantilever transfer function is approximately flat within this frequency range. Both $|\mathcal{X}|$ and $\theta_{\mathcal{X}}$ are much more corrugated at lower temperatures as the quality factors of mechanical components of the AFM increase. Assuming that $\mathcal{X}(\omega)$ is flat leads to a false interpretation of the drive signal acquired during an experiment. Our choice for using a logarithmic scale for $|\mathcal{X}|$ is important and justified elsewhere (see supplementary material, Sec. 2[44]).

II. MOTIVATION

Figure 1 displays a measurement of the transfer function of the piezoacoustic excitation system $\mathcal{X}(\omega)$, which describes how the piezoelectric transducer converts the drive voltage of the AGC into an effective force felt by the cantilever tip. This measurement was acquired by piezoacoustically driving the cantilever well below resonance where its transfer function is nearly flat and the driven cantilever response reflects changes in $\mathcal{X}(\omega)$. Figure 1 demonstrates that $\mathcal{X}(\omega)$ is far from flat in vacuum environments: hardware components mechanically coupled to the cantilever and piezoelectric transducer cause spurious resonances. In fact $\mathcal{X}(\omega)$ can be more corrugated in vacuum than in liquid environments, where it is typically referred to as the "forest of peaks" (see supplementary material, Sec. 1[41]). Furthermore, cooling the vacuum AFM to 77 K greatly accentuates features in $\mathcal{X}(\omega)$, as seen in Fig. 1; just as the cantilever quality factor Q increases, the quality factor of each spurious resonance also increases. These measurements of the phase $\theta_{\mathcal{X}}$ and amplitude $|\mathcal{X}|$ components of $\mathcal{X}(\omega)$ clearly demonstrate that both carry a strong frequency dependence. This has profound effects on FM-AFM measurements, as described in the following paragraphs.

The frequency dependence of $\theta_{\mathcal{X}}$, commonly assumed negligible, affects the tracking of the cantilever resonance frequency and thus modifies the measured frequency shift $\Delta\omega$ caused by conservative interactions with the sample.[42,43] This problem disappears as $Q \to \infty$ (see supplementary material, Sec. 2[44]), such that the effect of $\theta_{\mathcal{X}}$ can usually be neglected when the conservative force is calculated from $\Delta\omega$ in vacuum experiments where Q is large. However, it is important to note that the cantilever phase is *not* kept constant in the presence of a nonflat $\theta_{\mathcal{X}}$, regardless of Q. This is explained by the fact that the cantilever self-oscillates by positive feedback, such that the total phase around the self-excitation loop is always an integer multiple of -360°. If $\theta_{\mathcal{X}}$ varies by 10° upon some frequency shift, the cantilever phase will change by -10° to compensate. This fact holds even if the phase spectrum of the self-excitation electronics is flat compared to $\theta_{\mathcal{X}}$, as was verified on our system (see supplementary material, Sec. 4[45]). Driving a cantilever off resonance is less efficient, resulting in an increase of the drive amplitude necessary to maintain a constant oscillation amplitude. Importantly, this increase in drive amplitude is *not* related to tip-sample dissipative processes—it is purely instrumental.

The amplitude spectrum $|\mathcal{X}|$ does not affect the tracking of the cantilever resonance, however, it determines the efficiency for driving the cantilever at any given frequency. If $|\mathcal{X}|$ increases by 10% upon some frequency shift $\Delta\omega$, the drive amplitude will decrease by 10% simply to maintain a constant cantilever amplitude. Again, this decrease in drive amplitude is *not* related to tip-sample dissipative processes.

These heuristic explanations suggest that $\theta_{\mathcal{X}}$ and $|\mathcal{X}|$ must be considered when deriving the relationship between the drive amplitude and the damping due to tip-sample interaction. In other words, the drive-amplitude signal is expected to have a frequency dependence which must be corrected.

III. THEORY

This section presents the derivation which relates the drive amplitude to the tip-sample damping in FM-AFM in vacuum environments. Alternatively, this derivation can also be performed in the time-domain based on the approach of Hölscher *et al.*;[46] see supplementary material, Sec. 3.[47]

To high accuracy, a cantilever in vacuum environments can be modeled as a damped harmonic oscillator with a transfer function $\mathcal{C}(\omega)$ in units of m/N, which describes the response of the cantilever to a driving force exerted by the piezoacoustic excitation system. The amplitude component of $\mathcal{C}(\omega)$ is defined by (see Appendix)

$$|\mathcal{C}(\omega)| = -\frac{\sin\theta_{\mathcal{C}}(\omega)}{\omega \times \gamma}, \tag{1}$$

where $\theta_{\mathcal{C}}(\omega)$ is the phase spectrum of the cantilever, and γ is the damping (in Ns/m). Although this form of the transfer function is mathematically identical to the more conventional form, it provides a more useful way to describe the cantilever in the context of FM-AFM as it allows us to directly distinguish how changes in phase, drive frequency, and damping affect the cantilever amplitude response.

With this definition, the cantilever response before any tip-sample interaction is simply

$$|\mathcal{C}(\omega_s)| = -\frac{\sin\theta_{\mathcal{C}s}}{\omega_s \times \gamma_s}, \tag{2}$$

where $\theta_{\mathcal{C}s}$, ω_s, and γ_s are the phase of the cantilever, the self-excited oscillation frequency, and the damping; the

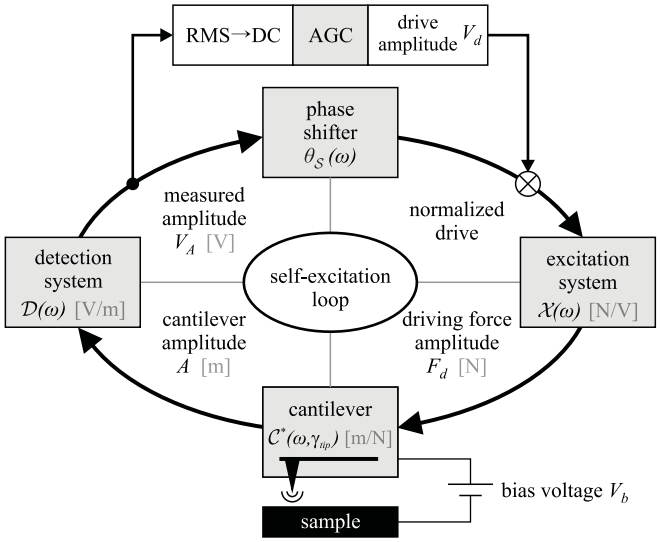

FIG. 2. The transfer functions comprising the self-excitation loop are represented as four grey boxes. The evolution of the self-excitation signal is described within the loop, along with units. The cantilever tip interacts with the sample; the bias voltage V_b between the two is adjustable. The AGC maintains a constant cantilever amplitude A by modulating the drive amplitude V_d; this is valid if the amplitude response of the detection system $|\mathcal{D}|$ is flat, as assumed through this article (dropping this assumption leads to a more complicated derivation[40]). The derivation in this article also assumes that self-excitation electronics ($\theta_{\mathcal{D}} + \theta_S$) have flat phase spectra, where $\theta_{\mathcal{D}}$ is the phase spectrum of the detection system.

subscript "s" denotes measurements taken at the start of the experiment before any tip-sample interaction occurs. The intrinsic cantilever damping γ_s is typically estimated by $\gamma_s \approx k/Q\omega_s$, where k and Q are the stiffness and quality factor of the unperturbed cantilever.

During the experiment, the cantilever transfer function (see Fig. 2) undergoes perturbation due to tip-sample conservative interactions, causing the self-excited oscillation frequency ω to vary. Also, the perturbed cantilever damping becomes $\gamma = \gamma_s + \gamma_{\text{tip}}$, where the additional damping γ_{tip} relates to the tip-sample dissipative interactions. As described in the previous section, the phase of the cantilever $\theta_{\mathcal{C}}(\omega)$ varies to compensate for changes in the excitation system phase response $\Delta\theta_{\mathcal{X}}(\omega)$. In the limit that the self-excitation electronics respond instantly, the cantilever phase is $\theta_{\mathcal{C}}(\omega) = \theta_{\mathcal{C}s} - \Delta\theta_{\mathcal{X}}(\omega)$, where the convention $\Delta\theta_{\mathcal{X}}(\omega_s) = 0^\circ$ is adopted for simplicity. Finally, from Eq. (1), the resulting perturbed cantilever amplitude transfer function becomes

$$|\mathcal{C}^*(\omega,\gamma_{\text{tip}})| = -\frac{\sin\left(\theta_{\mathcal{C}s} - \Delta\theta_{\mathcal{X}}(\omega)\right)}{\omega \times (\gamma_s + \gamma_{\text{tip}})}. \tag{3}$$

Note that $\theta_{\mathcal{C}s}, \theta_{\mathcal{X}}, \gamma_s$ can be measured before the experiment, and the self-excited oscillation frequency ω is measured during the experiment; therefore, γ_{tip} is the only unknown variable remaining to fully define $|\mathcal{C}^*(\omega,\gamma_{\text{tip}})|$.

In order to maintain a constant cantilever oscillation amplitude, the AGC adjusts the drive amplitude to account for changes in the amplitude response of the piezoacoustically driven cantilever $|\mathcal{X}| \times |\mathcal{C}^*(\omega,\gamma_{\text{tip}})|$. Measuring the drive amplitude during the experiment allows determining γ_{tip} as follows.

For a given drive amplitude V_d, the resulting cantilever oscillation amplitude A can be calculated by

$$A = V_d \times |\mathcal{X}| \times |\mathcal{C}|, \tag{4}$$

as can be understood from Fig. 2. This equation holds under the approximation that the detection system, which converts the cantilever displacement into a measurable voltage, has a frequency independent (flat) transfer function. This approximation is usually valid in vacuum environments[48] and is assumed herein. Throughout the whole experiment, A is kept constant by the AGC such that

$$\underbrace{V_d \times |\mathcal{X}(\omega)| \times |\mathcal{C}^*(\omega,\gamma_{\text{tip}})|}_{during\ the\ experiment} = \underbrace{V_s \times |\mathcal{X}(\omega_s)| \times |\mathcal{C}(\omega_s)|}_{start\ of\ the\ experiment}, \tag{5}$$

where V_s is the drive amplitude measured at the start of the experiment. Rearranging Eq. (5) results in

$$\Lambda = \frac{V_d}{V_s} = \left|\frac{\mathcal{X}(\omega_s)}{\mathcal{X}(\omega)}\right| \times \left|\frac{\mathcal{C}(\omega_s)}{\mathcal{C}^*(\omega,\gamma_{\text{tip}})}\right|, \tag{6}$$

where the normalized drive-amplitude signal Λ is defined for the convenience of avoiding units of volts. Notice that the drive signal Λ changes as a function of $|\mathcal{X}|$, which can be measured before or after the experiment, as will be thoroughly described in the next section. Both $|\mathcal{C}|$s are defined by Eqs. (2) and (3) with γ_{tip} as the only remaining unknown variable. Solving Eq. (6) allows us to infer the tip-sample damping γ_{tip} from the measured drive signal Λ by

$$\gamma_{\text{tip}} = \gamma_s\left(\frac{\Lambda}{ネ} - 1\right), \tag{7}$$

where ネ [the Japanese katakana symbol pronounced "ne"] is defined as

$$ネ(\omega) = \underbrace{\left|\frac{\sin(\theta_{\mathcal{C}s} - \Delta\theta_x(\omega))}{\sin(\theta_{\mathcal{C}s})}\right|^{-1}}_{\theta-factor} \underbrace{\left|\frac{\mathcal{X}(\omega)}{\mathcal{X}(\omega_s)}\right|^{-1}}_{x-factor} \underbrace{\left(\frac{\omega}{\omega_s}\right)}_{\sim 1}. \tag{8}$$

As can be understood from Eq. (7), ネ is the unitless calibration factor that corrects for the frequency dependence of the drive signal Λ, which otherwise can be mistaken for tip-sample damping. Note that for a purely conservative interaction, the drive-amplitude signal varies as $\Lambda = ネ$, which correctly results in $\gamma_{\text{tip}} = 0$ if processed by Eq. (7). Incorrectly assuming a constant $\mathcal{X}(\omega)$ by omitting ネ in Eq. (7) results in nonzero damping $\gamma_s\left(ネ - 1\right)$, which is designated as "apparent damping." In other words, apparent damping in the context of this article refers to the interpretation of the frequency dependence (ネ) of the drive signal using standard FM-AFM theory[4,32,49] rather than Eq. (7).

In Eq. (8) ネ is broken down into the θ-factor ("phase factor") and $\mathcal{X}$-factor ("excitation factor"), which describe how the drive-signal calibration is affected by a nonflat $\theta_{\mathcal{X}}$ and $|\mathcal{X}|$, respectively. These two factors were heuristically described in the Motivation section. Finally, we henceforth

omit the ω/ω_s factor from the discussion because it is usually two to three orders of magnitude smaller than the $\mathcal{X}$-factor in vacuum environments.

In most FM-AFM experiments, the accuracy in determining γ_{tip} is limited by the accuracy and precision in measuring $\not\asymp$, consisting of $|\mathcal{X}|$, $\theta_{\mathcal{X}}$, and $\theta_{\mathcal{C}s}$. This will be investigated in the following sections.

Before proceeding, we note that tip-sample dissipated power P_{tip} is proportional to γ_{tip} within the approximation $\omega/\omega_s \sim 1$, such that

$$P_{\text{tip}} = P_s\left(\frac{\Lambda}{\not\asymp} - 1\right), \tag{9}$$

where the starting cantilever dissipated power P_s is typically approximated by $P_s \approx \frac{1}{2}k\omega_o A^2/Q$.

IV. CHARACTERIZING THE EXCITATION SYSTEM

This section presents the protocol used to measure the piezoacoustic excitation transfer function $\mathcal{X}$, which is subsequently used to determine the starting phase of the cantilever $\theta_{\mathcal{C}s}$.

Piezoacoustically driving the cantilever and recording its response inevitably leads to the combined transfer function $\mathcal{XC}$ of the cantilever and the excitation system, as can be understood from Fig. 2. However, by independently measuring the cantilever transfer function $\mathcal{C}$, the $\mathcal{X}$ can be isolated by division. Applying a small amplitude AC bias voltage between the cantilever and sample results in an electrostatic driving force.[50] By sweeping the frequency of this AC bias, the transfer function of the cantilever $\mathcal{C}$ can be measured across any desired frequency range. This independent measurement of $\mathcal{C}$ allows the isolation of $\mathcal{X}$, as shown in Fig. 3. Note that the electrostatic excitation transfer function is assumed flat for this measurement.

For technical clarity, the exact protocol used to obtain the data in Fig. 3 is now explicitly outlined:

(i) Self-excite the cantilever with an AGC amplitude set point of 1.6 nm and adjust the phase shifter to minimize the drive amplitude (*the self-excited oscillation frequency becomes 156.30 kHz*).

(ii) Engage the tip-sample distance feedback controller with a frequency shift set point of −10 Hz after applying a 2 V tip-sample DC bias (*this approaches the tip to 10–20 nm above the sample*).

(iii) Disable the tip-sample distance feedback to fix the tip-sample distance.

(iv) Set the tip-sample bias to 10 V, thereby shifting the self-excited oscillation frequency to 155.92 kHz. (*This optional step reduces the necessary dynamic range necessary to perform the measurements in steps vi and vii and may reduce the effects of tip-sample drift on the estimation of $\mathcal{X}$ in step viii.*)

(v) Disable cantilever self-excitation.

(vi) Measure the transfer function $\mathcal{XC}$ by piezoacoustically driving the cantilever (V_d) and measuring the cantilever response (V_A) across [156.00 kHz, 156.33 kHz] (*this frequency range was selected to cover the frequency range used throughout the actual experiment*).

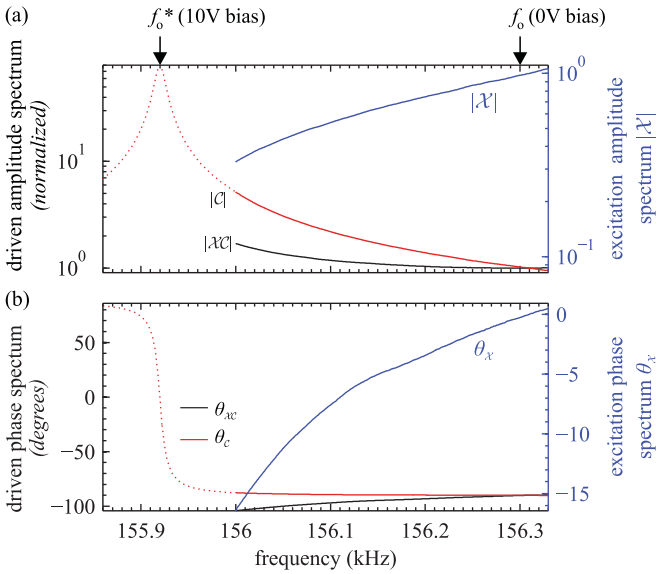

FIG. 3. (Color online) On the primary axes (black), the driven transfer functions of the cantilever for both the piezoacoustic ($\mathcal{XC}$) and the electrostatic ($\mathcal{C}$) methods of excitation are plotted in their (a) amplitude and (b) phase components. For this measurement, a ∼10 V bias was applied to the cantilever to shift the resonance frequency to below 156 kHz, whereas this measurement was only taken above 156 kHz: this reduces the necessary dynamic range for measuring $\mathcal{C}$ and $\mathcal{XC}$ because the measurement is taken where $\mathcal{C}$ is flatter. The dotted lines are extrapolated and only plotted for clarity. Dividing these transfer functions results in the piezoacoustic transfer function $\mathcal{X} = \mathcal{XC}/\mathcal{C}$, plotted on the secondary axes (blue/gray). The resonance frequency at the zero contact potential difference is labeled f_o, which corresponds to a null frequency shift in Fig. 4.

(vii) Measure the transfer function $\mathcal{C}$ by driving the cantilever with a tip-sample AC bias (V_b) and measuring the cantilever response (V_A) across [156.00 kHz, 156.33 kHz].

(viii) Infer the excitation transfer function by $\mathcal{X} = \mathcal{XC}/\mathcal{C}$ and calculate its magnitude $|\mathcal{X}|$ and phase $\theta_{\mathcal{X}}$.

This protocol was performed before *and* after the experiment, which is described in the next section, to verify that the transfer function $\mathcal{X}$ remained constant throughout the experiment. Linearity of the cantilever response was verified by acquiring both transfer functions at double the drive voltage.

Now, this measurement of $\mathcal{X}$ will be used to determine the starting phase of the cantilever $\theta_{\mathcal{C}s}$. Typically, the AFM user minimizes the drive amplitude at the start of the experiment by adjusting the phase shifter in an attempt to drive the cantilever on resonance. However, this method locates the maximum of $|\mathcal{XC}|$—not $|\mathcal{C}|$. Solving for $\partial\,|\mathcal{XC}|\,/\partial f = 0$ (see supplementary material, Sec. 5[51]) returns a starting cantilever phase

$$\theta_{\mathcal{C}s} = \text{atan}\frac{2Q}{(\alpha_{\mathcal{X}} f_o - 1)}, \tag{10}$$

where the normalized slope of the amplitude spectrum $\alpha_{\mathcal{X}} = |\mathcal{X}|^{-1}\,\partial\,|\mathcal{X}|\,/\partial f$ is evaluated at the resonance frequency f_o. Applying Eq. (10) to the data from Fig. 3 results in $\theta_{\mathcal{C}s} = -90.8^\circ \pm 0.5^\circ$. Note the Q dependence in Eq. (10); the commonly used drive-minimization method can misidentify

the true cantilever resonance by more than 10° in situations where $Q \sim 1000$ (see supplementary material, Sec. 5[51]).

Now $|\mathcal{X}|, \theta_{\mathcal{X}}$, and $\theta_{\mathcal{C}s}$ can be used to determine 禾, according to Eq. (8), allowing an accurate recovery of the damping signal in the following experiment.

V. EXPERIMENT

A home-built AFM[52] equipped with a piezoacoustic drive and a RF modulated interferometer[53] was cooled to ~77 K. A tip-side platinum-coated cantilever was approached to a height of a few nm above an octanethiol-covered gold surface. The cantilever resonance frequency was 156 301 Hz with a quality factor near 15 000. The cantilever oscillation amplitude was set to 1.6 nm. Sweeping the sample bias voltage resulted in a typical parabolic frequency shift signal vs voltage curve (not shown). In Fig. 4(a) the frequency-shift signal $\Delta\omega$ and drive-amplitude signal Λ are plotted against each other. The calculated 禾 is overlaid and shows that most of the drive signal Λ originates from coupling with $\Delta\omega$ due to the non-negligible frequency dependence of $\mathcal{X}(\omega)$. Note that no fitting parameters were used; 禾(ω) was fully determined before the experiment. Applying Eq. (7) recovers the true damping signal γ_{tip}, plotted in Fig. 4(b), which is free of apparent damping. There is no measurable damping in between 0 Hz and −200 Hz. Beyond −200Hz, true damping is observed only at a positive bias voltage, providing the evidence that γ_{tip} is not caused by coupling with $\Delta\omega$. The exact cause of the polarity dependence of this dissipation is currently under investigation. Clearly, assuming a flat $\mathcal{X}(\omega)$ would have resulted in an overwhelming amount of apparent damping, which would have affected our interpretation of the tip-sample physics. It is instructive to note

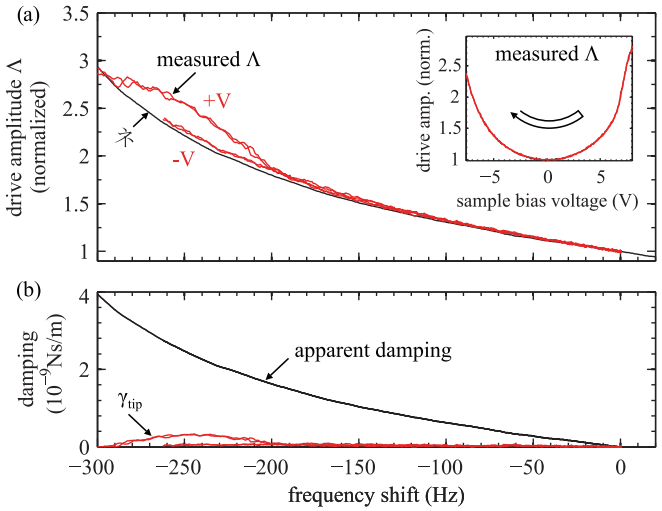

FIG. 4. (Color online) (a) The normalized drive amplitude Λ was measured while sweeping the sample bias voltage twice, as shown in the inset, and the same data is replotted vs measured frequency shift. The drive amplitude predicted for a conservative interaction (禾) is plotted and shows that most of the measured drive-amplitude signal is an instrumental artifact. (b) Using Eq. (7), the damping was recovered (γ_{tip}). Assuming a flat piezoacoustic excitation transfer function would have resulted in additional apparent damping, also plotted, and the additional true damping (γ_{tip}) would have been overestimated by almost 3×.

that simply subtracting the background (禾) from the drive signal Λ to isolate the true damping would have overestimated γ_{tip} by nearly a factor of 3, because 禾 follows a multiplicative, not additive, relationship with Λ, as seen in Eq. (7).

We now investigate the dominant cause of the frequency dependence of 禾. In our particular experiment, the $\mathcal{X}$-factor dominated 禾. The θ-factor only began to affect 禾 noticeably beyond −250 Hz and represented only 5% of the frequency dependence of 禾 at −300 Hz. This is due to the highly nonlinear behavior of the sine function in Eq. (8), which governs the impact of $\theta_{\mathcal{X}}$ on the drive signal Λ. Small phase deviations about $\theta_{\mathcal{C}s} = -90°$ have no measurable impact on 禾, because the sine function remains fairly flat. Once the cantilever phase deviates by more than ±10° from resonance, the θ-factor becomes noticeable.

VI. CHARACTERIZATION OF SEVERAL AFMS

This single experiment was adequate in demonstrating the utility of Eq. (7). However, properly characterizing six AFMs across the [60, 140] kHz bandwidth (see supplementary material, Sec. 7[54]) allows us to make more a general statement about the frequency dependence of the drive amplitude in FM-AFM. Although AFMs should be characterized on an *ad hoc* basis to determine their susceptibility to apparent damping, the following investigation allows us to discuss the general impact this source of apparent damping has had on different types of FM-AFM experiments in vacuum.

The figure of merit which quantifies the impact of the $\mathcal{X}$-factor is the normalized derivative of the amplitude transfer function $\alpha_{\mathcal{X}}$, defined in Eq. (10). Assigning $\alpha_{\mathcal{X}}$ units of %/10 Hz, which are equal to kHz^{-1} used previously,[39] describes this derivative as *the percentage change in the drive amplitude Λ for a 10 Hz frequency shift due to a conservative interaction*. In other words, $\alpha_{\mathcal{X}}$ summarizes the coupling between Λ and $\Delta\omega$ caused by the $\mathcal{X}$-factor. Note that $\alpha_{\mathcal{X}}$ was in between 2.5%/10 Hz and 6.5%/10 Hz for the data in Fig. 4, which led to significant apparent damping (up to 3× the intrinsic cantilever damping).

Our study of six AFMs suggests that $|\alpha_{\mathcal{X}}| > 1\%/10$ Hz should be commonly observed at 300 K on most vacuum AFMs. We have noticed that AFMs for which the cantilever is epoxied directly to the piezoelectric transducer have lower $|\alpha_{\mathcal{X}}|$ values. Figure 1 is representative of the excitation transfer function of such an AFM which has a slow-varying $|\mathcal{X}|$ that is characterized by a small number of resonances at 300 K. In general, the coupling value $\alpha_{\mathcal{X}}$ is as likely to be negative as positive. However, if there is a large mechanical resonance just above the typical operating frequency, an AFM user can expect a consistently positive apparent damping for negative frequency shifts. This would be the case, for example, if experiments were always performed around 85 kHz on our system at 300 K (see Fig. 1). On the other hand, AFMs with intricate cantilever holders, where the piezoelectric transducer is far from the cantilever, have an $|\mathcal{X}|$ that is highly corrugated due to the multitude of hardware components that are acoustically driven along with the cantilever (see supplementary material, Sec. 7[55]). Such an AFM can have $|\alpha_{\mathcal{X}}| > 3\%/10$ Hz for every tenth experiment performed at 300 K. Negative and positive coupling values $\alpha_{\mathcal{X}}$ are expected

to be equally likely, even between cantilevers with similar resonant frequencies.

The magnitude of the θ-factor depends on the slope of the phase transfer function $\beta_{\mathcal{X}}$, in units of $^\circ/10$ Hz. The discussion about $\alpha_{\mathcal{X}}$ in the previous paragraph qualitatively applies to $\beta_{\mathcal{X}}$, although typically the value of $\beta_{\mathcal{X}}$ (in $^\circ/10$ Hz) is roughly half the value of $\alpha_{\mathcal{X}}$ (in $\%/10$ Hz). Whereas the previous discussion concerning $\alpha_{\mathcal{X}}$ was independent of $\beta_{\mathcal{X}}$, the reverse is not true: a nonzero $\alpha_{\mathcal{X}}$ causes the starting phase of the cantilever $\theta_{cs} \neq -90^\circ$ and affects the impact that $\beta_{\mathcal{X}}$ has on the θ-factor, as can be understood from Eq. (8). The quantitative effects of a nonzero $\beta_{\mathcal{X}}$ on the drive signal are highly nonlinear, far from intuitive, and should be assessed on an *ad hoc* basis.

As shown in Fig. 1, the excitation transfer function $\mathcal{X}(\omega)$ has a strong temperature dependence. The $\mathcal{X}(\omega)$ of our home-built AFM was tested at 300, 77, and 4 K, with $|\alpha_{\mathcal{X}}|$ values larger than 0.4, 2.6, and $10\%/10$ Hz, respectively, affecting one tenth of the studied frequency range. The corresponding values of $|\beta_{\mathcal{X}}|$ were 0.2, 1.3, $5^\circ/10$ Hz. Roughly speaking, the problem of apparent damping is 25× larger at 4 K than it is at 300 K on our system. These observations are consistent with previous reports of exceedingly large apparent dissipation occurring at low temperatures.[29]

VII. SIMULATIONS

In this section, we discuss different experiments performed using FM-AFM to gauge the impact of the piezoacoustic excitation transfer function characterized in the previous section. The first subsection elaborates on the quantitative and qualitative effects of apparent damping in force spectroscopy. The second subsection deals with apparent damping observed in constant frequency shift FM-AFM imaging.

A. Force spectroscopy

The difference in apparent damping between room temperatures and cryogenic temperatures is not only quantitative. Whereas $\alpha_{\mathcal{X}}$ and $\beta_{\mathcal{X}}$, defined in the previous section, are typically fairly constant for a single experiment performed at 300 K, they can change dramatically as a function of frequency during a single experiment at 77 K, and especially at 4 K, because $\mathcal{X}(\omega)$ can be highly corrugated within a frequency window as small as 100 Hz.

The excitation system transfer function was acquired at 4 K just above the cantilever resonance of ∼157.5 kHz. Figure 5(a) shows one of the many mechanical resonances which afflict $\mathcal{X}$. Note that such mechanical resonances are plentiful even though the cantilever is glued directly to the piezoelectric transducer—inevitably, the cantilever is mechanically coupled to all the AFM hardware and its countless resonances. Figure 5(b) demonstrates that recording a transfer function of the driven cantilever ($\mathcal{XC}$) does *not* provide a clear indication that the cantilever is above or near a mechanical resonance, especially if the amplitude transfer function is plotted on a linear scale (see supplementary material, Sec. 2[44]).

In Fig. 5(c) a drive signal Λ was simulated assuming a purely conservative electrostatic interaction for both cantilevers defined in Fig. 5(b). The maximum frequency shift was -50 Hz, corresponding to a bias voltage of $\pm 5V$. The

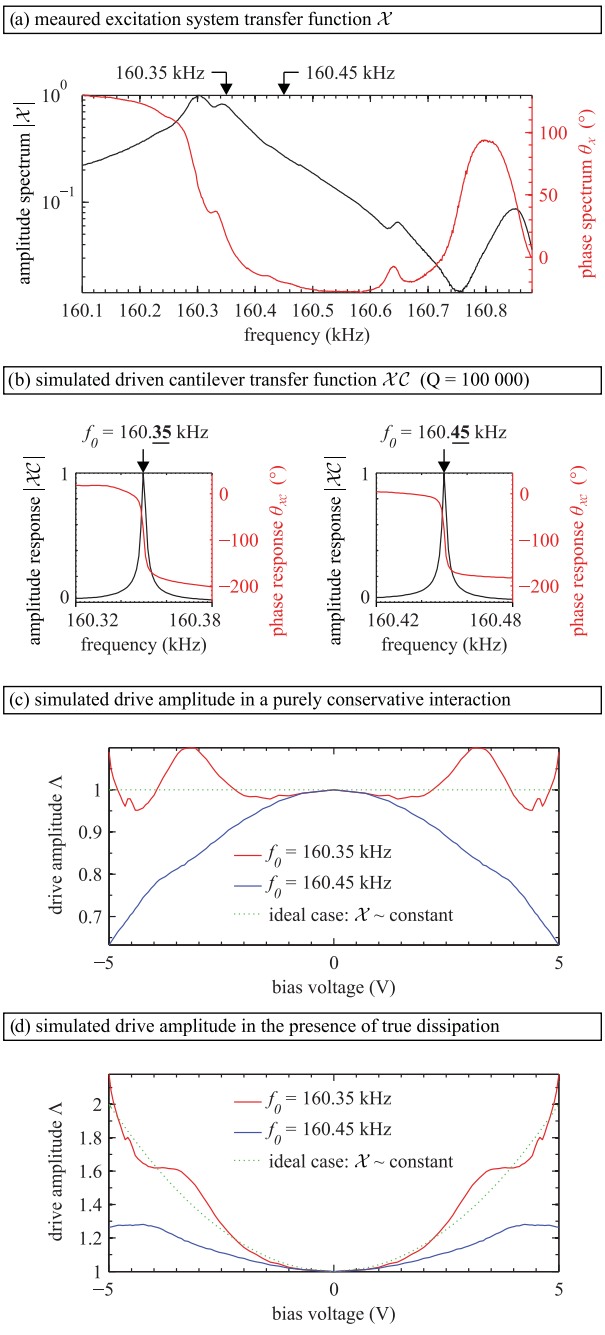

FIG. 5. (Color online) (a) The excitation system transfer function $\mathcal{X}(\omega)$ was measured at 4 K. (b) The driven cantilever response is modeled for both resonance frequencies indicated by arrows in (a). In either case, the driven transfer function does not seem problematic because the high Q value (10^5) of the cantilever provides a seemingly clean driven response. (c) An experiment is simulated for both cantilevers in (b), assuming a purely conservative electrostatic interaction with a quadratic dependence $\Delta f \sim V^2$; the ±5 V bias voltage corresponds to a frequency shift of -50 Hz. The dotted line represents the ideal case where the excitation transfer function is flat. (d) The same experiment is simulated by assuming a true tip-sample dissipation, which scales as $\gamma_{\text{tip}} \sim V^2$. At ±5 V bias, the tip-sample damping is equal to the intrinsic cantilever damping in this simulation. Clearly, the drive-amplitude signal strongly depends on $\mathcal{X}(\omega)$.

large variations and multiple peaks in the drive signal are representative of what we observe most of the time in our experiments at 4 K. Combined with Fig. 4, this simulation illustrates that the frequency dependent calibration (𝒦) of the drive amplitude can increase, decrease, or be highly corrugated as a function of frequency.

In the simulated data starting at 160.45 kHz, 𝒦 was dominated by the $\mathcal{X}$-factor (by >98%). However, for the data starting at 160.35 kHz, the θ-factor exceeded the $\mathcal{X}$-factor at frequency shifts beyond -45 Hz. The high Q-factor of the cantilever (10^5) ensured that the drive-minimization method accurately set the starting cantilever phase near -90° within 1°, but the steep phase spectrum of the excitation system ($\langle\beta_{\mathcal{X}}\rangle$avg $= -8.4^\circ/10$ Hz) caused the cantilever phase to reach $\theta_{\mathcal{C}} = -132.0^\circ$ at a frequency shift of -50 Hz. Operating the cantilever off resonance, at -132.0°, results in a θ-factor equal to 1.35. Note that measuring the phase response of the driven cantilever using a lock-in amplifier[56] would *not* identify the problem. In fact, a lock-in amplifier measures the combined phase response of the excitation system and the cantilever $\theta_{\mathcal{XC}}$ such that $\theta_{\mathcal{X}}$ and $\theta_{\mathcal{C}}$ can vary wildly during an experiment despite an ideal phase-locked loop (PLL) maintaining a constant $\theta_{\mathcal{XC}}$.

On many systems, "negative apparent damping" corresponding to $\Lambda < 1$, seen in Fig. 5(c), is rarely or never observed. The reason for this is demonstrated by the following simulation. Figure 5(d) represents the same simulation of an electrostatic interaction as shown in Fig. 5(c), however a nonzero tip-sample damping γ_{tip} was modeled as $\gamma_{\text{tip}} \sim V^2$, where V is the bias voltage (Joule heating, for example, follows this quadratic dependence[36,57]). The magnitude of the true damping was arbitrarily adjusted such that $\gamma_{\text{tip}} = \gamma_s$ at $\pm 5V$ bias voltage. For these conditions, the drive amplitude remains above 1; nevertheless, 𝒦 affects the drive amplitude by the same factor as in the absence of true damping. This can severely distort the drive-amplitude signal by introducing features that do not relate to tip-sample physics or by skewing the power-law behavior between $(\Lambda - 1)$ and the bias voltage V, for example. The power-law behavior within the $\pm 3V$ bias range in Fig. 5(d) is closer to V^4 than to V^2 by virtue of 𝒦.

B. Imaging

FM-AFM is most often used for acquiring images by raster scanning the sample and maintaining a constant frequency shift set point Δf_{set} by adjusting the tip-sample distance accordingly. In the ideal case where Δf_{set} remains perfectly constant throughout the experiment, 𝒦 will remain constant and therefore apparent damping will affect the entire drive-amplitude image by a constant factor. However, the ideal condition of a constant Δf_{set} is usually not fulfilled in practice, even if the PLL and AGC parameters are set to their optimal values (PLL locking time = 0.35 ms; AGC response time = 2 ms as defined in Ref. 29).

Figure 6 illustrates an atomic step edge and the resulting frequency-shift deviation despite imaging with a typical imaging speed (10 nm/s) and ideal PLL parameters.[29] Assuming that the amplitude transfer function of the excitation system has a slope $\alpha_{\mathcal{X}} = \pm 3\%/10$ Hz, which is expected to occur on our commercial AFM every tenth experiment at 300 K (see

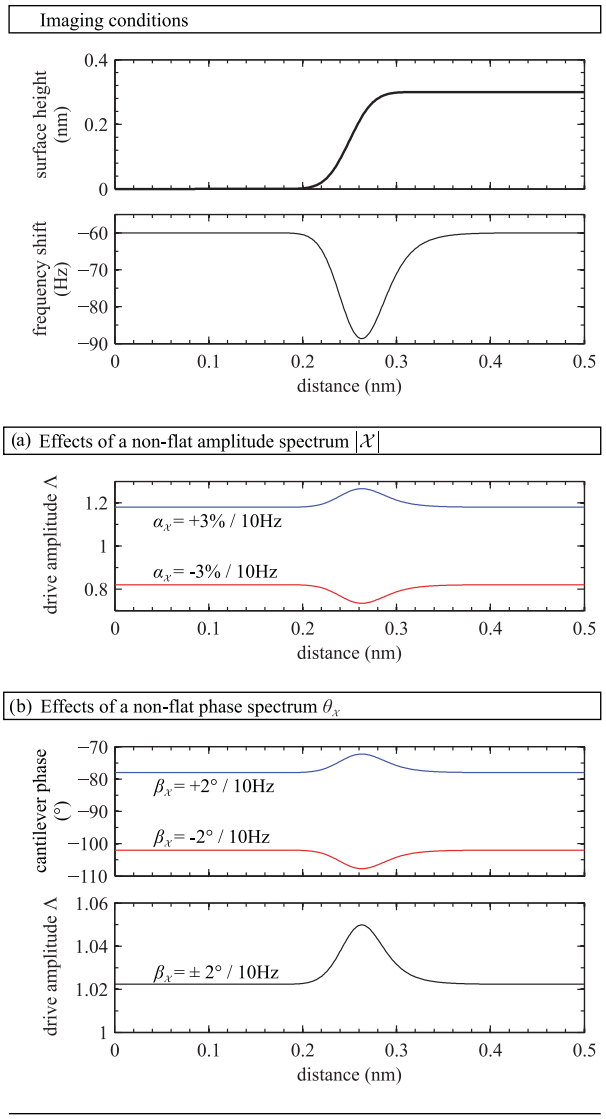

FIG. 6. (Color online) A step edge was modeled as shown. The scanning speed was set to 10 nm/s and the frequency-shift set point $\Delta f_{\text{set}} = -60$ Hz. The optimal, but finite, locking time of the PLL (0.35 ms) results in a transient frequency-shift deviation of nearly -30 Hz, as determined by Nony *et al.*[29] (a) If the amplitude spectrum of the excitation system has a slope of $\alpha_{\mathcal{X}} = \pm 3\%/10$ Hz, the drive amplitude will shift considerably upon approach to the surface and additionally during the transient frequency-shift deviation from set point. (b) If the phase spectrum of the excitation system has a slope $\beta_{\mathcal{X}} = \pm 2^\circ/10$ Hz, the cantilever phase will deviate from -90°, even if the PLL is ideal. This results in a positive drive-amplitude deviation.

supplementary material, Sec. 7[55]), the transient frequency-shift deviation will cause the drive amplitude to vary by nearly $\pm 9\%$, as seen in Fig. 6(a). If the true tip-sample damping at the step edge is much smaller than the cantilever intrinsic damping, a change in $|\mathcal{X}|$ in between experiments can lead to contrast inversion in between two drive-amplitude images. This can occur after a change in temperature, for example, or if cantilevers with different resonant frequencies are used.

Figure 6(b) demonstrates the situation where only the phase spectrum is nonflat with a slope of $\beta_{\mathcal{X}} = \pm 2^\circ/10$ Hz, which is expected to occur on our commercial AFM every tenth

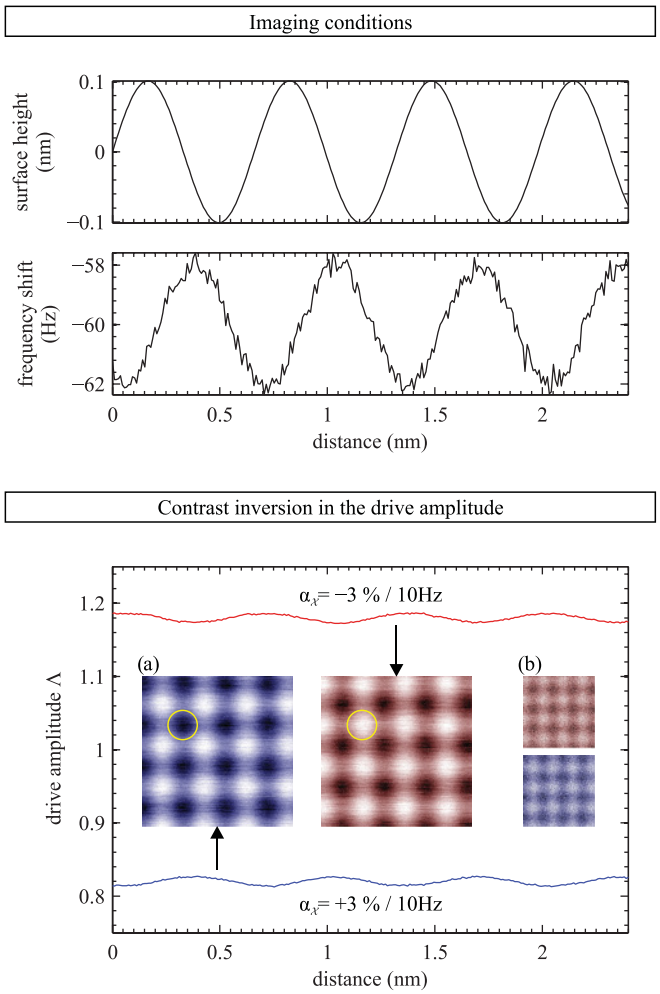

FIG. 7. (Color online) Atomic-scale corrugation of KBr was modeled as having 0.1 nm amplitude and a spatial wavelength of 0.66 nm. The scanning speed was set to 7 nm/s and the frequency shift set point $\Delta f_{\text{set}} = -60$ Hz. Despite accurate topography tracking (not shown), the frequency shift oscillates around the set point by ± 2 Hz, as simulated by Nony *et al.*[29] It is assumed that there is no measurable tip-sample dissipation. The drive-amplitude oscillations due to the coupling to the frequency shift were calculated from the frequency-shift signal according to coupling values $\alpha_{\mathcal{X}} = \pm 3\%/10$ Hz. Both drive-amplitude signals clearly demonstrate that contrast inversion can occur solely due to the excitation system transfer function $|\mathcal{X}|$. (a) The simulated drive-amplitude images assume that only cantilever thermal noise and the detection noise n_d affect the measurements. (b) The second pair of images shows that contrast inversion is still observable in the case where the electronic noise reaches 2% of the drive-amplitude signal (cantilever parameters: $k = 40$ N/m, $f_0 = 160$ kHz, $Q = 15\,000$, $A = 10$ nm, $n_d = 40\,fm/\sqrt{\text{Hz}}$).

experiment at 300 K. Both cases, positive and negative, result in an increase of the drive amplitude because driving the cantilever off resonance in either direction is less efficient. Despite ideal PLL parameters, the cantilever is driven at $\pm 12^\circ$ off resonance when the frequency is kept constant ($\Delta f_{\text{set}} = -60$ Hz) and reaches $\pm 18^\circ$ at the step edge resulting in a significant contrast in the drive amplitude.

Contrast inversion can also occur at the atomic scale due to apparent damping. However, due to the smaller magnitude of the apparent damping in this context, noise becomes a key consideration when assessing the experimental relevance of the problem.

When scanning KBr with atomic resolution at a scan speed of 7 nm/s with optimized PLL parameters and a set point $\Delta f_{\text{set}} = -60$ Hz, the deviations from the set point reach values of roughly ± 2 Hz despite accurate topography tracking.[29] As seen in Fig. 7, these deviations are observable well above the frequency noise computed using the theory of Kobayashi *et al.*,[58] assuming a detection noise of 40 fm/$\sqrt{\text{Hz}}$. Assuming that only this detection noise and thermal noise of the cantilever limit the ability of the AGC to maintain a constant cantilever oscillation amplitude, contrast inversion in the drive amplitude should be clearly visible between situations where $|\mathcal{X}|$ has either $\alpha_{\mathcal{X}} = \pm 3\%/10$ Hz. This is illustrated by the simulated drive-amplitude images in Fig. 7(a).

On many systems the measured drive-amplitude signal is limited by other noise sources, such as additional electronic noise. It has been well established that drive amplitude contrast on the order of 2% or higher is experimentally relevant on most systems because it can exceed true tip-sample damping as well as instrumental noise.[7,11,29] Adding white noise with a standard deviation $\sigma = 0.02$ to the simulated drive-amplitude images, shown in Fig. 7(b), demonstrates that atomic-scale contrast inversion caused by piezoacoustic excitation should be resolvable above noise on most systems.

VIII. SUMMARY

This section summarizes the effects of the transfer function of piezoacoustic excitation system $\mathcal{X}(\omega)$ on dissipation experiments. The frequency dependence of $\mathcal{X}(\omega)$ couples the detected cantilever frequency shift $\Delta\omega$ to the AGC drive amplitude Λ, typically referred to as the "dissipation" or "damping" signal. Neglecting this frequency dependence of Λ leads to apparent damping and therefore inaccurate interpretation of measured FM-AFM data. The frequency-dependent changes in the drive-amplitude calibration are described by the unitless $\nvDash(\omega)$, which should be measured before or after the experiment to allow for the correction of this apparent damping. The dominant component of $\nvDash$, for most experiments, is the $\mathcal{X}$-factor, which accounts for changes in the amplitude spectrum $|\mathcal{X}|$ of the excitation system. Further in this section, the effects of the θ-factor caused by the nonflat phase spectrum $\theta_{\mathcal{X}}$ will also be summarized.

Dissipation spectroscopy is the technique most strongly affected by this source of apparent damping, particularly at cryogenic temperatures where the $\mathcal{X}$-factor can be corrugated on a frequency window as small as 100 Hz. Depending on the shape of the transfer function, this may result in qualitatively inconsistent damping measurements for different cantilevers, unless corrected for. That is, repeated experiments may result in drive-amplitude profiles with different shapes effectively only reflecting the shape of $|\mathcal{X}|$, as opposed to changes in tip-sample damping. At room temperature, the $\mathcal{X}$-factor is nearly always smooth across a 100 Hz bandwidth, with a shallower amplitude-spectrum slope $\alpha_{\mathcal{X}}$. Although apparent damping is much less severe at room temperature, it can

significantly affect sensitive dissipation experiments where the tip-sample damping is much smaller than the cantilever intrinsic damping.

For applications using constant frequency shifts with some set point Δf_{set}, such as typical FM-AFM topography imaging, apparent damping can appear in two ways. Each cantilever will have a different drive-amplitude calibration at identical Δf_{set} because of differences in their $\mathcal{X}$-factor; if left uncorrected, this can lead to quantitatively variable-dissipation measurements taken at identical Δf_{set} with different cantilevers and may prevent drawing conclusions about dissipative mechanisms under study. In the second scenario, transient deviations from a constant set point Δf_{set}, due to the finite response time of the PLL or distance regulation feedback, may cause experimentally significant apparent damping, for example, at step edges. This can cause inconsistent results between cantilevers, or even for the same cantilever if operated at a different Δf_{set}. Atomic-scale contrast inversion in the drive amplitude is also likely to occur because coupling constants on the order of $\pm 3\%/10\,\text{Hz}$, which can be observed on most AFMs even at room temperature, cause apparent damping, which exceeds the true tip-sample damping and instrumental noise.

Although the θ-factor rarely dominates the $\mathcal{X}$-factor in typical experiments (see supplementary material, Sec. 6[54]), the former should not be neglected. At cryogenic temperatures, a very corrugated phase spectrum $\theta_{\mathcal{X}}$ implies that carefully setting the cantilever on resonance away from the surface (at $\Delta f = 0\,\text{Hz}$) does not ensure proper resonance tracking during the experiment; once $\Delta f_{\text{set}} \neq 0\,\text{Hz}$, the cantilever will be driven off resonance and even small modulations of the cantilever phase may significantly enhance apparent damping by a large θ-factor contribution. At room temperature, the much shallower phase spectrum reduces the magnitude of this problem. However, the drive-minimization method is more likely to fail because of a lower cantilever Q-factor which can misidentify the true cantilever resonance by more than 10° in certain situations. This could lead to a significant θ-factor even for small frequency shifts.

IX. CONCLUSION

In FM-AFM operated with a piezoacoustically excited cantilever, the AGC drive-amplitude signal can only be accurately converted into a damping or dissipation signal after measuring the transfer function $\mathcal{X}(\omega)$ of the piezoacoustic excitation system. This measurement allows the decoupling of conservative and dissipative forces by correcting for the frequency dependence of the drive amplitude, which does not relate to tip-sample damping. Using standard FM-AFM theory leads to apparent damping in force spectroscopy as well as topography imaging, thereby potentially altering the quantitative and qualitative interpretation of the tip-sample physics. We have demonstrated a nondestructive and robust method which enables measuring $\mathcal{X}(\omega)$, thereby eliminating apparent damping which can dominate the true tip-sample damping signal.

The impact of apparent damping depends on numerous parameters, such as frequency shift, Q-factor, temperature, feedback parameters, and most importantly the details of the mechanical construction of the AFM. Due to the complexity of the problem, the impact of apparent damping must be considered on an *ad hoc* basis for any particular experiment performed at any temperature. Conclusive statements about qualitative and quantitative FM-AFM dissipation studies (using a piezoacoustically excited cantilever) rely on a proper investigation of the piezoacoustic excitation system, as presented in this paper.

Whereas we are not denying that other studied sources of apparent damping can be significant, we have shown that the transfer function of the piezoacoustic excitation system accounts for a large part of the observed variability in reported dissipation experiments to date. Applying the methodology presented in this paper can reconcile many discrepancies between theory and experiment, which have thus far prevented advancement in FM-AFM dissipation applications and studies.

ACKNOWLEDGMENTS

A.L. would like to acknowledge the help and valuable discussions with Jeffrey Bates, Sarah Burke, Philip Egberts, Monserratt Lopez-Ayon, William Paul, Antoine Roy-Gobeil, Antoni Tekiel, and Jessica Topple, as well as guidance from Roland Bennewitz through existing literature. A.L. also greatly acknowledges his memorable stay in Kyoto, Japan, where the study of FM-AFM in liquid environments with Hirofumi Yamada, Kei Kobayashi, and Daniel Kiracofe was an indispensable ingredient for this study in vacuum environments. Funding from NSERC, FQRNT and CIfAR are gratefully acknowledged.

APPENDIX : REPARAMETRIZING THE CANTILEVER TRANSFER FUNCTION

A cantilever interacting with a sample can be described as a damped harmonic oscillator with two time-varying parameters. The choice of these parameters is somewhat arbitrary. Typically, the amplitude transfer function is defined by the resonance frequency ω_0 and the quality factor Q as in

$$|\mathcal{C}(\omega|\omega_o, Q)| = \frac{1}{k}\sqrt{\frac{1}{[1-(\omega/\omega_o)^2]^2 + (\omega/\omega_o Q)^2}}, \tag{A1}$$

with its associated phase transfer function

$$\theta_{\mathcal{C}}(\omega) = \tan^{-1}\left\{-\frac{\omega/\omega_o}{Q[(1-(\omega/\omega_o)^2]}\right\}, \tag{A2}$$

where k is the cantilever stiffness, which remains constant. This is not a very useful parameterization of the cantilever transfer function in FM-AFM because the perturbed cantilever resonance due to tip-sample interaction is unknown to the AFM user during the experiment. Furthermore the quality factor Q carries an intrinsic dependence on the variable resonance frequency.

Using the rules of trigonometry, Eq. (A2) can be rewritten as

$$\sin\theta_{\mathcal{C}}(\omega) = -\frac{\omega/\omega_o Q}{\sqrt{[(1-(\omega/\omega_o)^2]^2 + (\omega/\omega_o Q)^2}}, \tag{A3}$$

which, combined with Eq. (A1), results in

$$|\mathcal{C}(\omega|\omega_o, Q)| = -\frac{\omega_o Q}{k}\frac{\sin\theta_{\mathcal{C}}(\omega)}{\omega}. \tag{A4}$$

Using the well-known relations

$$Q = \frac{m\omega_o}{\gamma} \quad \text{and} \quad k = m\omega_o^2, \tag{A5}$$

the cantilever amplitude transfer function can be reparametrized to

$$|\mathcal{C}(\omega|\theta_{\mathcal{C}}, \gamma)| = -\frac{\sin\theta_{\mathcal{C}}(\omega)}{\omega \times \gamma}. \tag{A6}$$

Note that Eq. (A6) is mathematically identical to Eq. (A1). This reparametrized version of the cantilever transfer function is useful for FM-AFM applications because it directly relates changes in phase, frequency, and damping to the amplitude response $|\mathcal{C}|$.

*aleks.labuda@gmail.com

[1] T. R. Albrecht, P. Grutter, D. Horne, and D. Rugar, J. Appl. Phys. **69**, 668 (1991).
[2] U. Dürig, O. Züger, and A. Stalder, J. Appl. Phys. **72**, 1778 (1992).
[3] U. Dürig, H. R. Steinauer, and N. Blanc, J. Appl. Phys. **82**, 3641 (1997).
[4] H. Hölscher, B. Gotsmann, W. Allers, U. Schwarz, H. Fuchs, and R. Wiesendanger, Phys. Rev. B **64**, 075402 (2001).
[5] Y. Sugimoto, M. Abe, S. Hirayama, N. Oyabu, O. Custance, and S. Morita, Nat. Mater. **4**, 156 (2005).
[6] Y. Sugimoto, S. Innami, M. Abe, Oscar. Custance, and S. Morita, Appl. Phys. Lett. **91**, 093120 (2007).
[7] T. Trevethan, L. Kantorovich, J. Polesel-Maris, and S. Gauthier, Nanotechnology **18**, 084017 (2007).
[8] H. Hölscher, B. Gotsmann, W. Allers, U. Schwarz, H. Fuchs, and R. Wiesendanger, Phys. Rev. Lett. **88**, 019601 (2001).
[9] S. A. Burke and P. Grütter, Nanotechnology **19**, 398001 (2008).
[10] Ch. Loppacher, M. Bammerlin, M. Guggisberg, S. Schär, R. Bennewitz, A. Baratoff, E. Meyer, and H.-J. Güntherodt, Phys. Rev. B **62**, 16944 (2000).
[11] M. Gauthier, R. Pérez, T. Arai, M. Tomitori, and M. Tsukada, Phys. Rev. Lett. **89**, 146104 (2002).
[12] T. Kunstmann, A. Schlarb, M. Fendrich, D. Paulkowski, Th. Wagner, and R. Möller, Appl. Phys. Lett. **88**, 153112 (2006).
[13] M. Guggisberg, Surf. Sci. **461**, 255 (2000).
[14] S. Molitor, P. Guthner, and T. Berghaus, Appl. Surf. Sci. **140**, 276 (1999).
[15] M. Fendrich, T. Kunstmann, D. Paulkowski, and R. Möller, Nanotechnology **18**, 084004 (2007).
[16] R. Hoffmann, M. Lantz, H. Hug, P. van Schendel, P. Kappenberger, S. Martin, A. Baratoff, and H.-J. Güntherodt, Phys. Rev. B **67**, 085402 (2003).
[17] R. Garcia, C. Gómez, N. Martinez, S. Patil, C. Dietz, and R. Magerle, Phys. Rev. Lett. **97**, 016103 (2006).
[18] T. Trevethan, Surf. Sci. **540**, 497 (2003).
[19] T. Trevethan and L. Kantorovich, Nanotechnology **16**, S79 (2005).
[20] T. Trevethan and L. Kantorovich, Nanotechnology **17**, S205 (2006).
[21] L. Kantorovich and T. Trevethan, Phys. Rev. Lett. **93**, 236102 (2004).
[22] S. Ghasemi, Stefan Goedecker, Alexis Baratoff, Thomas Lenosky, Ernst Meyer, and Hans Hug, Phys. Rev. Lett. **100**, 236106 (2008).
[23] M. Gauthier and M. Tsukada, Phys. Rev. B **60**, 11716 (1999).
[24] A Abdurixit, A. Baratoff, and E. Meyer, Appl. Surf. Sci. **157**, 355 (2000).
[25] T. Trevethan and L. Kantorovich, Nanotechnology **15**, S44 (2004).
[26] M. Gauthier and M. Tsukada, Phys. Rev. Lett. **85**, 5348 (2000).
[27] L. Kantorovich, Surf. Sci. **521**, 117 (2002).
[28] L. Kantorovich, Phys. Rev. B **64**, 245409 (2001).
[29] L. Nony, A. Baratoff, D. Schär, O. Pfeiffer, A. Wetzel, and E. Meyer, Phys. Rev. B **74**, 235439 (2006).
[30] G. Langewisch, H. Fuchs, and A. Schirmeisen, Nanotechnology **21**, 345703 (2010).
[31] S. Morita, R. Wiesendanger, and E. Meyer, *Noncontact Atomic Force Microscopy* (Springer, Berlin, 2002), p. 399.
[32] J. P. Cleveland, B. Anczykowski, A. E. Schmid, and V. B. Elings, Appl. Phys. Lett. **72**, 2613 (1998).
[33] L. Cockins, Y. Miyahara, S. D Bennett, A. A Clerk, S. Studenikin, P. Poole, A. Sachrajda, and P. Grutter, PNAS **107**, 9496 (2010).
[34] S. D. Bennett, L. Cockins, Y. Miyahara, P. Grütter, and A. A. Clerk, Phys. Rev. Lett. **104**, 017203 (2010).
[35] L. Cockins, Y. Miyahara, S. D. Bennett, A. A. Clerk, and P. Grutter, submitted (2011).
[36] M. Kisiel, E. Gnecco, U. Gysin, L. Marot, S. Rast, and E. Meyer, Nat. Mater. **10**, 119 (2011).
[37] M. Ternes, C. González, C. Lutz, P. Hapala, F. Giessibl, P. Jelínek, and A. Heinrich, Phys. Rev. Lett. **106**, 016802 (2011).
[38] N. Oyabu, P. Pou, Y. Sugimoto, P. Jelinek, M. Abe, S. Morita, R. Pérez, and Ó. Custance, Phys. Rev. Lett. **96**, 106101 (2006).
[39] R. Proksch and S. V Kalinin, Nanotechnology **21**, 455705 (2010).
[40] A. Labuda, K. Kobayashi, D. Kiracofe, K. Suzuki, P. H. Grütter, and H. Yamada, AIP Adv. **1**, 022136 (2011).
[41] See Supplemental Material at http://link.aps.org/supplemental/10.1103/PhysRevB.84.125433 in Sec. 1 for the "forest of peaks."
[42] K. Kobayashi, H. Yamada, and K. Matsushige, Rev. Sci. Instrum. **82**, 033702 (2011).
[43] W. Hofbauer, *Scanning Probe Microscopy—Dynamic Force Microscopy in Liquid Media,* (World Scientific, Singapore, 2010), Chapter 7, pp. 137–163.
[44] See Supplemental Material at http://link.aps.org/supplemental/10.1103/PhysRevB.84.125433 in Sec. 2 for the illusory nature of the "forest of peaks."
[45] See Supplemental Material at http://link.aps.org/supplemental/10.1103/PhysRevB.84.125433 in Sec. 4 for the investigation of electronic phase shifts.
[46] H. Hölscher, B. Gotsmann, W. Allers, U. Schwarz, H. Fuchs, and R. Wiesendanger, Phys. Rev. B **64**, 075402 (2001).

[47]See Supplemental Material at http://link.aps.org/supplemental/10.1103/PhysRevB.84.125433 in Sec. 3 for the derivation of FM-AFM dissipation theory in the time-domain.

[48]In vacuum environments, cantilever frequency shifts are typically much smaller than in liquid environments, and band-pass filters are typically not necessary to obtain stable self-excitation. Therefore, the frequency dependence of the detection electronics is usually negligible. Dropping this assumption leads to a more elaborate derivation.[40]

[49]U. Dürig, Surf. Interface Anal. **27**, 467 (1999).

[50]B. Terris, J. Stern, D. Rugar, and H. Mamin, Phys. Rev. Lett. **63**, 2669 (1989).

[51]See Supplemental Material at http://link.aps.org/supplemental/10.1103/PhysRevB.84.125433 in Sec. 5 for the bias in the drive-minimization method.

[52]M. Roseman and P. Grütter, Rev. Sci. Instrum. **71**, 3782 (2000).

[53]D. Rugar, H. J. Mamin, and P. Guethner, Appl. Phys. Lett. **55**, 2588 (1989).

[54]See Supplemental Material at http://link.aps.org/supplemental/10.1103/PhysRevB.84.125433 in Sec. 6 for the X-factor Vs Θ-factor.

[55]See Supplemental Material at http://link.aps.org/supplemental/10.1103/PhysRevB.84.125433 in Sec. 7 for the "forest of peaks" growing larger in vacuum.

[56]A. E. Gildemeister, T. Ihn, C. Barengo, P. Studerus, and K. Ensslin, Rev. Sci. Instrum. **78**, 013704 (2007).

[57]O. Pfeiffer, L. Nony, R. Bennewitz, A. Baratoff, and E. Meyer, Nanotechnology **15**, S101 (2004).

[58]K. Kobayashi, H. Yamada, and K. Matsushige, Rev. Sci. Instrum. **80**, 043708 (2009).